Cylindrical brushes with ionized side chains: Scaling theory revisited

Ekaterina B Zhulina, Oleg V. Borisov

Soft Matter d3sm00727h

We have presented the graphical abstract image and text for your article below. This briefly summarises your work, and will be presented with your article online.

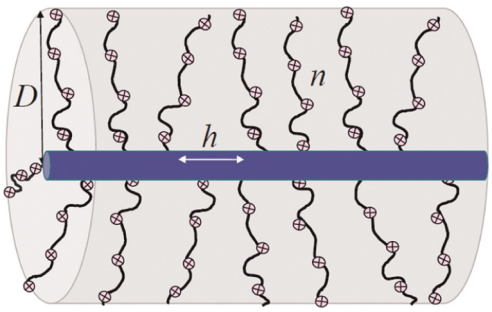

Cylindrical brushes with ionized side chains: Scaling theory revisited

Ekaterina B. Zhulina and Oleg V. Borisov

We revisit the classic scaling model of a cylindrical polyelectrolyte (PE) brush focusing on molecular brushes with stiff backbones and dispersions of polymer-decorated nanorods.

Q1 Q2 Q3

Please check this proof carefully. Our staff will not read it in detail after you have returned it.

Please send your corrections either as a copy of the proof PDF with electronic notes attached or as a list of corrections. **Do not edit the text within the PDF or send a revised manuscript** as we will not be able to apply your corrections. Corrections at this stage should be minor and not involve extensive changes.

Proof corrections must be returned as a single set of corrections, approved by all co-authors. No further corrections can be made after you have submitted your proof corrections as we will publish your article online as soon as possible after they are received.

Please ensure that:

- The spelling and format of all author names and affiliations are checked carefully. You can check how we have identified the authors' first and last names in the researcher information table on the next page. **Names will be indexed and cited as shown on the proof, so these must be correct.**
- Any funding bodies have been acknowledged appropriately and included both in the paper and in the funder information table on the next page.
- All of the editor's queries are answered.
- Any necessary attachments, such as updated images or ESI files, are provided.

Translation errors can occur during conversion to typesetting systems so you need to read the whole proof. In particular please check tables, equations, numerical data, figures and graphics, and references carefully.

Please return your **final** corrections, where possible within **48 hours** of receipt following the instructions in the proof notification email. If you require more time, please notify us by email to softmatter@rsc.org.

Funding information

Providing accurate funding information will enable us to help you comply with your funders' reporting mandates. Clear acknowledgement of funder support is an important consideration in funding evaluation and can increase your chances of securing funding in the future.

We work closely with Crossref to make your research discoverable through the Funding Data search tool (http://search.crossref.org/funding). Funding Data provides a reliable way to track the impact of the work that funders support. Accurate funder information will also help us (i) identify articles that are mandated to be deposited in **PubMed Central (PMC)** and deposit these on your behalf, and (ii) identify articles funded as part of the **CHORUS** initiative and display the Accepted Manuscript on our web site after an embargo period of 12 months.

Further information can be found on our webpage (http://rsc.li/funding-info).

What we do with funding information

We have combined the information you gave us on submission with the information in your acknowledgements. This will help ensure the funding information is as complete as possible and matches funders listed in the Crossref Funder Registry.

If a funding organisation you included in your acknowledgements or on submission of your article is not currently listed in the registry it will not appear in the table on this page. We can only deposit data if funders are already listed in the Crossref Funder Registry, but we will pass all funding information on to Crossref so that additional funders can be included in future.

Please check your funding information

The table below contains the information we will share with Crossref so that your article can be found *via* the Funding Data search tool. **Please check that the funder names and grant numbers in the table are correct and indicate if any changes are necessary to the Acknowledgements text.**

Funder name	Funder's main country of origin	Funder ID (for RSC use only)	Award/grant number
Russian Science Foundation	Russia	501100006769	20-13-00270

Researcher information

Please check that the researcher information in the table below is correct, including the spelling and formatting of all author names, and that the authors' first, middle and last names have been correctly identified. **Names will be indexed and cited as shown on the proof, so these must be correct.**

If any authors have ORCID or ResearcherID details that are not listed below, please provide these with your proof corrections. Please ensure that the ORCID and ResearcherID details listed below have been assigned to the correct author. Authors should have their own unique ORCID iD and should not use another researcher's, as errors will delay publication.

Please also update your account on our online manuscript submission system to add your ORCID details, which will then be automatically included in all future submissions. See here for step-by-step instructions and more information on author identifiers.

First (given) and middle name(s)	Last (family) name(s)	ResearcherID	ORCID iD
Ekaterina B.	Zhulina	G-5177-2011	0000-0001-9139-3484
Oleg V.	Borisov	I-5177-2017	0000-0002-9281-9093

Queries for the attention of the authors

Journal: **Soft Matter**

Paper: **d3sm00727h**

Title: **Cylindrical brushes with ionized side chains: Scaling theory revisited**

For your information: You can cite this article before you receive notification of the page numbers by using the following format: (authors), Soft Matter, (year), DOI: 10.1039/d3sm00727h.

Editor's queries are marked on your proof like this Q1, Q2, etc. and for your convenience line numbers are indicated like this 5, 10, 15, ...

Please ensure that all queries are answered when returning your proof corrections so that publication of your article is not delayed.

Query reference	Query	Remarks
Q1	Have all of the author names been spelled and formatted correctly? Names will be indexed and cited as shown on the proof, so these must be correct. No late corrections can be made.	
Q2	Do you wish to indicate the corresponding author(s)? If so, please specify the corresponding author(s).	
Q3	Please check that the inserted Graphical Abstract image and text are suitable. If you provide replacement text, please ensure that it is no longer than 250 characters (including spaces). If you provide a replacement image, it can be in colour, at most 8 cm wide by 4 cm high (preferably a 600 dpi TIF file).	
Q4	A citation to Fig. 3 has been added here, please check that the placement of this citation is suitable. If the location is not suitable, please indicate where in the text the citation should be inserted.	
Q5	In the sentence beginning 'That is, the number. . .' a word or phrase appears to be missing after 'the number'. Please check and indicate the changes required.	
Q6	Please note that a conflict of interest statement is required for all manuscripts. Please read our policy on Conflicts of interest (http://rsc.li/conflicts) and provide a statement with your proof corrections. If no conflicts exist, please state that ''There are no conflicts to declare''.	
Q7	Have all of the funders of your work been fully and accurately acknowledged? If not, please ensure you make appropriate changes to the Acknowledgements text.	
Q8	Please indicate where ref. 29 should be cited in the text.	
Q9	The page numbers provided for ref. 29 appear to be incorrect. Please check and correct as necessary.	

Soft Matter

PAPER

Cylindrical brushes with ionized side chains: Scaling theory revisited

Cite this: DOI: 10.1039/d3sm00727h

Ekaterina B. Zhulina [a] and Oleg V. Borisov [ab]

Received 4th June 2023,
Accepted 11th October 2023

DOI: 10.1039/d3sm00727h

rsc.li/soft-matter-journal

We revisit the classic scaling model of a cylindrical polyelectrolyte (PE) brush focusing on molecular brushes with stiff backbones and dispersions of polymer-decorated nanorods. Based on the blob representation we demonstrate that similarly to the case of planar PE brushes, separation of intra- and intermolecular repulsions between charges leads to novel scaling regimes for cylindrical PE brushes in salt-added solution and a sharper decrease in its thickness *versus* salt concentration dependence. These theoretical predictions may inspire further comprehensive experimental research and computer simulations of synthetic and biopolyelectrolyte cylindrical brushes.

1 Introduction

Molecular brushes and polymer-decorated nanorods are widely examined theoretically and experimentally with the aim to advance functions of new materials, including thin films, bulk elastomers, and gels.

Branched polymers (molecular brushes) comprising a linear backbone and multiple side chains have remained the focus of ongoing research for a number of decades.[1–7] Intermolecular interactions between densely grafted side chains govern the specific properties of such macromolecules in solutions and bulk materials, as compared to linear polymers. The developed synthetic strategies: (i) ''grafting to'', (ii) ''grafting-through'', and (iii) ''grafting from'' provide a variety of branched architectures with the ''grafting from'' approach being most efficient to obtain macromolecules with long backbones and high grafting densities of side chains. The possibility to vary independently polymerization degrees (DPs) of the backbone and side chains, and grafting density of the pendants allows for control of the static and dynamic properties of graft polymers in solutions, gels, and bulk materials.[2,4,5] For example, self-organization of block copolymers with incompatible comb-like or bottlebrush blocks can be exploited for the fabrication of nanostructured materials with tissue-mimetic mechanical properties and structural colorations.[8–11]

Polyelectrolyte brushes can also mimic certain structural features of natural biological layers. In particular, charged cylindrical brushes could model aggrecans – essential components of cartilage in synovial joints,[12] neurofilaments – building blocks of the cytoskeleton in axons of neurons,[13] and cylinder-like cilium decorated with polymeric mucins.[14]

Analytical[15] and self-consistent field numerical[16,17] theories as well as coarse-grained computer simulations[18–25] of branched macromolecules have established the relationships between macromolecular topology and experimentally accessible properties of materials comprising elastomers and hairy gels[26–28] composed of physically or chemically cross-linked bottlebrushes. However, a vast majority of the theoretical studies on bottlebrushes deal with neutral systems, while computational studies of molecular brushes with ionized grafts are relatively sparse.[30–32]

The first scaling models of polyelectrolyte (PE) brushes were developed in the 1990s.[33–37] They presumed stretching of polyions normally to the grafting surface, localization of their end-points in the vicinity of external brush boundaries, and laterally smeared distribution of charges all over the brush volume. The original models predicted three major PE brush regimes in all geometries: osmotic (at low salt concentration), salt-dominated (at intermediate salt concentrations), and quasi-neutral (at large amounts of salt with predominantly non-electrostatic monomer–monomer interactions). An additional, charged regime served as a narrow corridor separating individual polyions from osmotic brushes. The scaling models provided the power law dependences for the brush thickness and polymer density profile as functions of molecular parameters: degree of ionization and molecular weight of the tethered polyions, their grafting density, radius of grafting surface, and solvent strength. While in the osmotic regime the thickness of the PE brush does not depend (in scaling terms) on the geometry of the underlying substrate, in the salt-dominated regime the exponent in the dependence of the brush thickness on the salt concentration depends on the system geometry, and is specified as $(j + 2)^{-1}$ with

[a] Institute of Macromolecular Compounds of the Russian Academy of Sciences, St. Petersburg, Russia. E-mail: oleg.borisov@uiv-pau.fr
[b] Institut des Sciences Analytiques et de Physico-Chimie pour l'Environnement et les Matériaux, UMR 5254 CNRS UPPA, Pau, France

dimensionality j = 1, 2, 3 for planar, cylindrical, and spherical PE brushes, respectively.[37]

Further extensions/modifications in the PE brush theory followed various paths, including analytical Poisson–Boltzmann frameworks with the account of rigidity, polydispersity and architecture of the tethered polyions, size and valence of the mobile ions, the solvent structure (see, *e.g.* the review in ref. 38 *etc.*), and extensive computer simulations (see *e.g.* ref. 23, 39, and 40 and references therein). The studies pointed at a more complex structure of PE brushes compared to neutral counterparts, and provided many fine details of polyion organization in thin surface layers. Distinction between intra-chain and inter-chain electrostatic repulsions in planar PE brushes[41] demonstrated that while osmotic and quasi-neutral regimes are not affected by separation of these interactions, the salt-dominated regime is noticeably modified. Instead of single exponent −1/3 in the salt dependence of the brush thickness, the planar PE brush exhibits three subregimes with consecutive exponents −1/3, 0, and −3/7, prior to becoming quasi-neutral.

The rest of the paper is organized as follows: in Section 2, we formulate the model of a cylindrical PE brush with a rigid backbone, and briefly summarize the scaling results for isolated polyions in aqueous solution. In Section 3 we review the scaling model of the salt-free cylindrical PE brush. In Section 4 we consider the effect of salt on the thickness of the cylindrical PE layer with emphasis on novel regimes that arise due to separation of intra- and intermolecular repulsions. In Section 5 we discuss the results and we outline our conclusions in Section 6.

2 Model

A cylindrical PE brush consists of a rigid backbone (cylindrical core) decorated with long side chains (polycations) attached to the core at multiple grafting points. This model applies to bottlebrush macromolecules comprising a stiff main chain with DP $M \gg 1$, and flexible linear side chains each with DP n, regularly tethered at a distance h along the backbone, as well as to polymer-decorated nanorods with long flexible ligands (Fig. 1). The backbone has radius ρ while the flexible side chains are assumed to have monomer unit size a, and Kuhn segment length $\simeq a$. The linear distance h between neighboring grafting points is related to the radius ρ of the core and the chain grafting density σ as $h = (2\pi\rho\sigma)^{-1}$. The side chains are permanently charged with the degree of ionization $0 \le \beta \le 1$. If $\beta = 0$, the grafts are neutral while at $\beta = 1$ each monomer unit in the side chain has elementary charge e. The Bjerrum length $l_B = e^2/(\varepsilon k_B T)$ is assumed to be on the order of a (*i.e.*, for $l_B \approx$ 0.7 nm in aqueous solution with dielectric permeability $\varepsilon \simeq 80$, ratio $l_B/a \simeq 1$). Each charged side chain produces βn mobile counterions distributed over the volume of the system that can also contain monovalent salt ions with concentration c_s. The latter specifies the Debye screening length as $r_D = (8\pi l_B c_s)^{-1/2}$. We consider close to theta solvent conditions with respect to the short-range van der Waals interactions between monomer units, corresponding to the predominance of ternary over binary contacts between monomers.

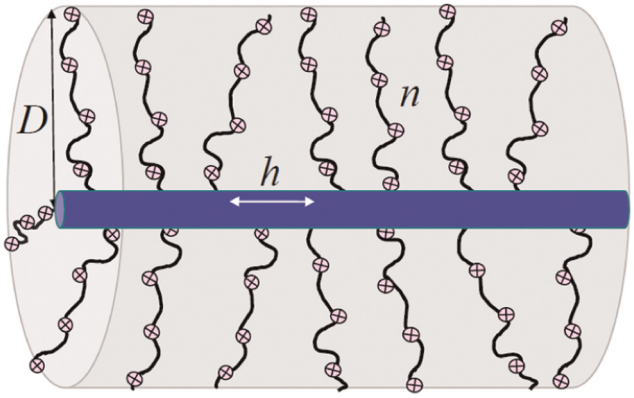

Fig. 1 Schematic of a cylindrical polycationic brush with DP n of tethered polyions and degree of ionization β (*i.e.*, with number $n\beta$ of charged monomer units per polyion, or equivalently, partial charge $e\beta$ per monomer unit), and linear distance h between neighboring grafts. Mobile ions are not shown.

The short-range repulsive interactions between neutral grafts ($\beta = 0$) cause elongation of the side chains when neighboring grafts start to overlap, $h \simeq R_G \simeq an^{1/2}$. In contrast to neutral side chains, polyelectrolyte grafts orient normally to the backbone prior to overlap due to the cumulative electric field created by the grafts. A similar effect was predicted for polyelectrolytes loosely tethered to a planar surface that orient normally prior to overlap.[36] However, orientation of the charged grafts does not cause their elongation that typically starts when the average distance h between neighboring grafts becomes on the order of the average size $R_e(\beta,n)$ of an isolated side chain (graft). At this point, the elastic intramolecular force acting in the graft becomes comparable to the orientational electric force created by neighboring polyions, and we assimilate the condition

$$h \simeq R_e \tag{1}$$

for the onset of the side chain elongation.

According to the existing scaling models,[39] the average end-to-end distance R_e of an isolated charged polyion with DP n and degree of ionization β in aqueous solution with $\varepsilon \approx 80$ is specified as

$$R_e/a \simeq \begin{cases} \beta^{2/3} n u^{1/3} & \text{charged regime IS} \\ n^{1/2} & \text{quasi-neutral regime G} \end{cases} \tag{2}$$

where we have introduced the conventional notation $u = l_B/a \simeq 1$. The first line in eqn (2) corresponds to the charged polyion with the degree of ionization $\beta > (l_B/a)^{1/2} n^{-3/4} \simeq n^{-3/4}$ in dilute salt-free solution. Its size R_e is specified by the balance of repulsive Coulomb force acting between $Q = \beta n$ elementary charges on the polyion ($\sim Q^2 l_B/R_e^2$) and the Gaussian elastic force ($\sim R_e/a^2 n$). The macromolecule is envisioned as a sequence of $n_e \simeq n\beta^{4/3}$ electrostatic blobs with size

$$\xi_e \simeq a\beta^{-2/3} u^{-1/3} \tag{3}$$

each, and the Coulomb repulsion energy $\sim k_BT$ per blob. At $\beta < n^{-3/4}$ the repulsion between charges is insufficient to stretch the polyion, and it retains the Gaussian size $R_G \simeq an^{1/2}$ (second line in eqn (2)).

3 Polyelectrolyte cylindrical brush in salt-free solution

Under theta-solvent conditions, the average brush thickness D (proportional to the average end-to-end distance of the side chain) of a neutral (quasi-neutral) bottlebrush is specified by the balance between repulsive ternary monomer–monomer interactions with the third virial coefficient $\simeq a^6$ and the Gaussian elasticity of the side chains to give[37]

$$D_{qn} \cong a\frac{n^{2/3}}{h^{1/3}} \tag{4}$$

The polymer volume fraction profile $c(r)$ in neutral bottlebrush yields

$$c_{qn}(r) \simeq \frac{a}{(hr)^{1/2}} \tag{5}$$

Eqn (5) suggests that side chains form the elastic blobs with size

$$\xi_{qn} \simeq (rh)^{1/2} \tag{6}$$

that densely fill the space (concentric cylindrical layers) in the brush. That is, area per chain $\simeq hr$ at distance r from the backbone equals the cross-sectional area of the blob, $hr \simeq \xi_{qn}^2$. Here and below, the subscript indicates the brush state (quasi-neutral qn, charged c, or osmotic osm).

In order to evaluate D and $c(r)$ in charged brushes, one has to account for the long-range electrostatic interactions between side chains. The scaling regimes of the charged cylindrical brush were originally discussed in the mean-field framework for charge distribution.[37] We briefly review here the relevant results.

The free energy F per chain of the bottlebrush with rodlike backbone comprises the elastic contributions $F_{elastic}$ due to stretching of the side chain (polyion), and the electrostatic free energy W due to the interactions between charges on polyions and counterions,

$$F = F_{elastic} + W$$

In the absence of salt, the polyion exhibits Gaussian elasticity on all length scales, and the elastic contribution

$$\frac{F_{elastic}}{k_BT} \simeq \frac{D^2}{a^2n} \tag{7}$$

The electrostatic contribution W has different forms depending on the values of h and β.

For sparsely tethered grafts and relatively small β (charged regime C), a cylindrical brush with backbone length L and linear charge density $\beta ne/h$ does not retain its counterions. In this case, mobile counterions spread almost uniformly over the volume per PE brush in the solution. At concentrations of PE brushes close to the overlap threshold ($\sim L^{-3}$), the major part of counterions is located outside of the brush with thickness $D \ll L$, making the brush almost net charged. Considering the PE brush as one plate of the cylindrical capacitor with linear charge density $\beta n/h$, and the second plate located at distance $\sim L$, the electrostatic free energy W per period of the brush can be evaluated as

$$\frac{W}{k_BT} \approx \frac{ua(\beta n)^2}{h}\ln\left(\frac{L}{D}\right) \tag{8}$$

For densely tethered and stronger charged grafts, the major part of counterions is retained inside the brush (osmotic regime O), making it almost electroneutral. In this case W is expressed *via* the translational entropy of entrapped counterions,

$$\frac{W}{k_BT} \approx \beta n\ln\left(\frac{\beta n}{hD^2c_s}\right) \tag{9}$$

Minimization of the total free energy F with respect to D with retention of only dominant terms leads to the power law dependences for the equilibrium thickness D of an ionic bottlebrush with a stiff backbone, collected in Table 1, together with the equilibrium parameters of the quasi-neutral brush and individual side chains.

In Fig. 2 we present the scaling-type diagram of states for such bottlebrushes in β,h coordinates. To the right of the boundary $h \simeq R_e$ marked by the dashed lines (eqn (2)), a cylindrical brush with a stiff backbone has non-overlapping side chains with an average end-to-end distance $D \simeq R_e$ if $h > R_e$ (regime IS) or $D \simeq R_G \simeq an^{1/2}$ (regime G). To the left of the dashed lines (at relatively large h), the brush is found either in charged (C) or quasi-neutral (QN) regimes. Notably, in the charged regime the C distance $h/\beta n$ remains larger than l_B. Similarly to planar brushes, regime C is a narrow intermediate regime separating isolated polyions from the osmotic brush.

In scaling terms, the onset of counterion condensation ($h/\beta n \simeq l_B$) occurs at the boundary between charged (C) and osmotic (O) regimes, in which the dominant part of counterions condense inside the volume of the brush. Specifics of the counterion distribution upon crossing the C–O boundary are beyond the scaling model adopted in this paper. However, smooth crossover of the brush thickness D at the C–O boundary suggests that the applied scaling model correctly accounts for the major brush rearrangement associated with counterion condensation.

Table 1 Equilibrium parameters of a cylindrical PE brush in various regimes of the diagram of states in Fig. 2

Regimes	D/a	$c(r)$
Charged (C)	$\beta u^{1/2}n^{3/2}(a/h)^{1/2}$	—
Osmotic (O)	$\beta^{1/2}n$	$\beta^{-1/2}(a^2/hr)$
Quasi-neutral (QN)	$n^{2/3}(a/h)^{1/3}$	$(a^2/hr)^{1/2}$
Isolated (IS)	$\beta^{2/3}u^{1/3}n$	$\beta^{-2/3}\,u^{-1/3}\,(a/r)^2$
Gaussian (G)	$n^{1/2}$	a/r

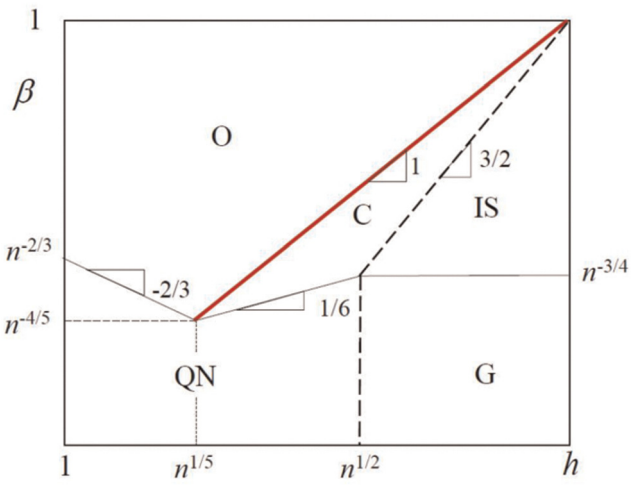

Fig. 2 Scaling-type diagram of states for a cylindrical PE brush in salt-free solution in β,h log–log coordinates, $l_B = a$. The red line $\beta = h/na$ corresponds to the onset of counterion condensation in the brush volume. Overlap thresholds for side chains, $h = R_e$, shown by dashed lines separate regimes of individual polyions (IS and G) from brush regimes (O,C,QN). Theta-solvent conditions with respect to short-range van der Waals monomer–monomer interactions.

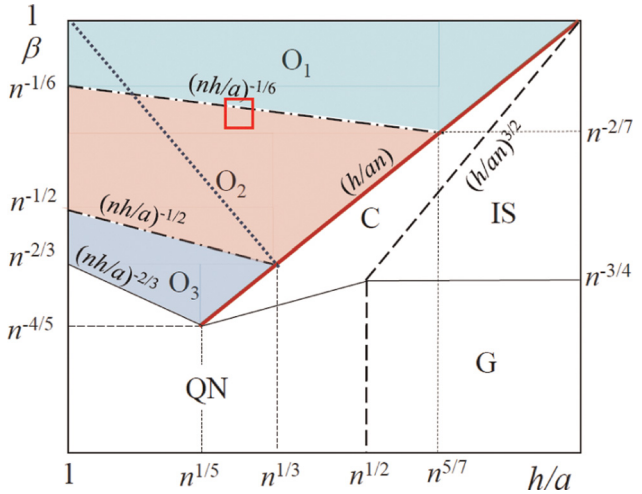

Fig. 3 Scaling-type diagram of states for a cylindrical PE brush in salt-free solution in, log–log coordinates. Notations are the same as in Fig. 2. Osmotic regime O is divided in sub-regimes: O_1 (shaded green), O_2 (shaded pink) and O_3 (shaded blue), each corresponding to a different sequence of power law dependences for brush thickness $D(c_s)$ depicted in Fig. 5. Equations for boundaries are indicated. The dotted line $\beta = (h/a)^{-2}$ separates states of osmotic brush with and without a quasi-neutral sublayer. The red square marks an area with $\beta = 0.25–0.38$ and $h/a = 3–4$ for pure NF_L.

In Fig. 3 the osmotic regime (O) in the diagram of states (the same as in Fig. 2) is divided into three subregimes with different colors. We explain this subdivision later.

3.1 Polymer volume fraction profile

Under conditions of the Gaussian elasticity for tethered polyions, the radial polymer density profile

$$c(r) \simeq \frac{a^3}{hr}\frac{\mathrm{d}n(r)}{\mathrm{d}r} \tag{10}$$

in the PE brush can be found by balancing the side chain tension,

$$t(r) \simeq k_B T \frac{\mathrm{d}r}{a^2 \mathrm{d}n(r)},$$

and the electrostatic force $f(r)$ acting at the chain segment $\mathrm{d}n(r)$.

In the osmotic regime O, $f(r)$ is specified by osmotic pressure $\Pi(r) = k_B T \beta c(r)$ of mobile counterions, to give

$$f(r) \simeq \Pi hr \simeq k_B T \beta \frac{\mathrm{d}n(r)}{\mathrm{d}r}$$

The force balance condition,

$$\frac{\mathrm{d}r}{a\mathrm{d}n} \simeq \beta^{1/2}, \tag{11}$$

indicates that side chains in the osmotic regime can be envisioned as strings of elastic blobs with size

$$\xi_{osm} \simeq a\beta^{-1/2}$$

oriented normally to the backbone. A similar structure of tethered polyions (strings of blobs with size $\xi_{osm} \simeq a\beta^{-1/2}$) has been predicted in planar and spherical osmotic brushes as well. The corresponding polymer density profile in a cylindrical brush yields

$$c_{osm}(r) \simeq \frac{a^2}{\beta^{1/2} hr} \tag{12}$$

Notably, a small fraction of counterions escapes from the brush in the osmotic regime O to conserve net charge density $q \simeq l_B^{-1} \simeq a^{-1}$ per unit length of the backbone. The fraction of escaped counterions is however much smaller compared to the fraction of retained counterions, $\simeq \beta n/h$, when $\beta \gg h/an$, which is in the middle of the osmotic regime O.

In the charged regime C, the polymer density profile in the cylindrical brush is not described by a single power law dependence. Conformations of tethered polyions with end-points fixed at the outer brush boundary have been addressed using the "capacitor" model.[42] It was demonstrated that in the equal stretching approximation for tethered polyions (that is, when the distribution of the chain-free end is approximated by the delta-function $\delta(r - D_c)$), the polymer density profile decays approximately as $c_c(r) \sim (r/D_c)$ in the inner part of the brush ($r/D_c \lesssim 0.5$) and exhibits a strong increase in the outer part of the brush ($r/D_c \gtrsim 0.5$) that does not obey power law dependence. If restriction on end-points of the side chains is relaxed, and they spread through the whole brush, the parabolic approximation for the electrostatic potential $\Psi(r)$ leads to the polymer density profile $c_c(r) \simeq (u\beta n)^{-2} a^{-3} = \text{const}$ everywhere inside the brush. Both approximations (*i.e.*, with pinched or unrestricted positions of end-points) provide the same scaling dependence for the brush thickness $D_c/a \simeq n^{3/2}\beta u^{1/2}/(h/a)^{1/2}$ with numerical prefactors on the order of unity, but lead to quite different patterns for the polymer density distribution $c_c(r)$. The account

of dead zone (which emerges in a cylindrical charged brush in the parabolic potential framework) performed along the lines in ref. 43 and 44 indicates no change in the power law dependence for D_c but leads to the logarithmic prefactor $\sim\log(D_c/a)$ in the free energy F_c per chain. In frames of the scaling approximation adopted here, logarithmic prefactors are omitted.

3.2 Internal blob structure of osmotic polyelectrolyte bottlebrush

In contrast to a planar brush of grafted polyions, the inner and outer parts of the cylindrical PE brush could be in different states. While the state of the main, outer sublayer is specified by the regime in the diagram of states in Fig. 2 (*e.g.* osmotic regime O with blob size ξ_{osm}), the state of the inner sublayer depends on the ratios between h, ξ_{osm} and ξ_{qn}.

If $h > \xi_{osm} \simeq a\beta^{-1/2}$, the strings of blobs with size ξ_{osm} start directly from the surface of the backbone (no inner sublayer), and the polymer density profile $c_{osm}(r)$ is given by eqn (12) in the whole body of the osmotic brush. If $h < \xi_{osm}$, the inner layer with radius r^* emerges while the outer sublayer still exhibits the osmotic regime at $r > r^*$.

If $h/a < n^{1/5}$, and $h < \xi_{osm}$, then the neighboring to regime O is quasi-neutral regime QN, and the inner layer constitutes the system of densely packed blobs whose size $\xi_{qn}(r)$ is given by eqn (6). The thickness of the inner sublayer r^* is specified as $\xi_{qn}(r^*) \simeq \xi_{osm}$ to give $r^* \simeq {\xi_{osm}}^2/h > \xi_{osm}$, with $r^* \ll D \simeq an\beta^{1/2}$ above the O–QN boundary, $\beta \simeq (nh/a)^{-2/3}$. In this range of parameters strings of osmotic blobs originate from the surface of the cylinder with radius r^*, while inside the inner sublayer the increasingly sized blobs are densely packed. An approach to boundary O–QN leads to the increase in $r^* \simeq D_{qn}$, and disappearance of the outer layer upon crossing the O–QN boundary. At $h/a > n^{1/5}$, condensation of counterions at the neighboring O–C boundary, makes it challenging to specify O–C transformation in scaling terms.

In Fig. 4 we schematically illustrate the blob structure of side chains in various regimes of the diagram in Fig. 2a: (a) in the osmotic regime O with $h > \xi_{osm}$ and no inner sublayer, (b) in the osmotic regime O with $h < \xi_{osm}$ and two-layer structure, and (c) regime I of individual polyions with $h > R_e$. Different blob colors correspond to different regimes: pink for ξ_e, green for ξ_{qn}, and yellow for ξ_{osm}.

In the following we focus on the osmotic regime O, which is the main regime of salt-free PE brushes in all geometries, and examine how additions of monovalent salt affect the thickness of the PE brush.

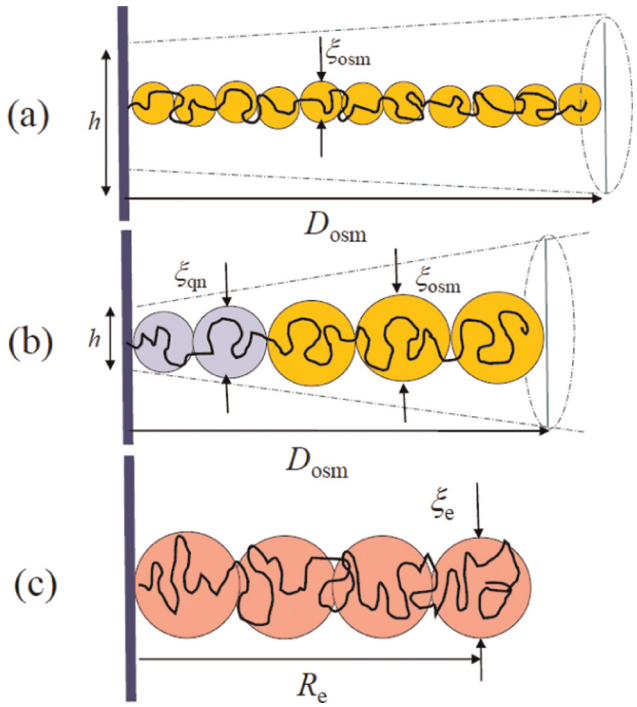

Fig. 4 Schematics of the blob structure in tethered polyions in salt-free solution: osmotic regime O with $\beta > (h/a)^{-2}$ (a) and $\beta < (h/a)^{-2}$ (b), and regime IS of individual polyions (c). Colors are: yellow for osmotic elastic blobs, ξ_{osm}, blue for quasi-neutral blobs, ξ_{qn}, and pink for electrostatic blobs, ξ_e.

4 Polyelectrolyte cylindrical brush in salt-added solution

In a cylindrical PE brush, the stretching force created by mobile ions decreases not only with increasing c_s but also with distance r from the backbone. In the scaling model, the area per chain $s(r)$ at distance r from the backbone increases as $s(r) \simeq hr$.

In the salt-added solution, tethered polyions are exposed to the differential osmotic pressure of mobile ions[45]

$$\frac{\Delta\Pi(r)a^3}{k_BT} = c_+(r) + c_-(r) - 2c_s = 2c_s\left(\sqrt{\left(\frac{\beta c(r)}{2c_s}\right)^2+1} - 1\right) \approx \begin{cases} \beta c(r) & \beta c(r) \gg c_s \\ \beta^2 c(r)^2/c_s & \beta c(r) \ll c_s \end{cases} \quad (13)$$

Here,

$$c_-(r) = c_s\left[\frac{\beta c(r)}{2c_s} + \sqrt{\left(\frac{\beta c(r)}{2c_s}\right)^2+1}\right] \approx \begin{cases} \beta c(r) & \beta c(r) \gg c_s \\ c_s(1+\beta c(r)/2c_s) & \beta c(r) \ll c_s \end{cases} \quad (14)$$

and

$$c_+(r) = c_s\left[-\frac{\beta c(r)}{2c_s} + \sqrt{\left(\frac{\beta c(r)}{2c_s}\right)^2+1}\right] \approx \begin{cases} {c_s}^2/\beta c(r) & \beta c(r) \gg c_s \\ c_s(1-\beta c(r)/2c_s) & \beta c(r) \ll c_s \end{cases} \quad (15)$$

are concentrations of mobile counterions and coions at distance r from the backbone, $\beta c(r)$ is the concentration of

immobile charges on polyions, and eqn (13) was derived assuming brush local electroneutrality, $c_-(r) \approx c_+(r) + \beta c(r)$.

The electrostatic stretching force per chain

$$\frac{f_\perp(r)}{k_B T} \simeq s(r)\Delta\Pi(r)/k_B T \simeq hr\Delta\Pi(r)/k_B T \qquad (16)$$

determines local tension $t(r)$ in polyions, and the polymer density profile $c(r)$.

A mean-field picture of the salt-dominated cylindrical brush[46] implies that charges on polyions and small mobile ions are uniformly spread throughout the brush to ensure the brush local electroneutrality. This approximation leads to a single power law dependence for the brush thickness D as a function of salt concentration c_s, $D \sim (\beta^2/c_s)^{1/4}$, which is obtained by balancing the Gaussian elasticity of polyions with differential osmotic pressure of salt ions.

As we demonstrate below, the account of intramolecular Coulomb repulsions localized on the polyion charges leads to novel regimes in the cylindrical brush behavior. Depending on the values of c_s, the polymer density distribution $c(r)$ and the brush thickness D demonstrate novel power law dependences. Below we discuss different regimes of PE cylindrical brush (indicated by subscripts I–V) in salt-added solution in detail.

4.1 Regime I: $0 < c_s < c_s^I$

The osmotic PE brush retains its size

$$D_I = D_{osm} \simeq a\beta^{1/2}n \qquad (17)$$

and the polymer density profile

$$c_I(r) = c_{osm}(r) \simeq \frac{a^2}{\beta^{1/2}hr} \qquad (18)$$

up to salt concentrations (volume fractions of salt ions) $c_s = c_s^I$ at which the concentration $\beta c_I(D_I)$ of counterions at the outer brush boundary ($r \simeq D_I$) becomes comparable to the concentration c_s of added salt ions,

$$c_s^I \simeq \beta c_I(D_I) \simeq \frac{a}{nh} \qquad (19)$$

The h-dependent contribution $F_{I,ion}$ to the electrostatic free energy per polyion is specified by the free energy of mobile ions (at fixed chemical potentials $\ln c_s$ of the ions in the solution). With the account of polymer density profile $c_I(r)$ in eqn (18),

$$\frac{F_{I,ion}}{k_B T} \simeq \int_a^{D_I} \beta c_I(r) \ln\left(\frac{\beta c_I(r)}{c_s}\right) a^{-3} s(r)\mathrm{d}r \approx \beta n \ln\left(\frac{a\beta}{nhc_s}\right) \qquad (20)$$

The derivative of F_I with respect to distance h between grafting points,

$$\frac{f_\parallel^I}{k_B T} = -\frac{1}{k_B T}\frac{\partial F_I}{\partial h} \simeq \frac{\beta n}{h} \qquad (21)$$

Specifies the lateral ion-induced electrostatic force $f_\parallel$ acting in the cylindrical core (in the backbone) in regime I.

4.2 Regime II: $c_s^I < c_s < c_s^{II}$

At $c > c_s^I$, the salt-dominated regime II starts to develop in the external brush sublayer, and differential osmotic pressure of mobile ions, $\Pi(r)a^3/k_B T$, changes there from $\beta c(r)$ to $\beta^2 c(r)^2/c_s$. Radius r_I of the inner osmotic sublayer is specified as $\beta c_I(r_I) \simeq c_s$ to give

$$r_I \simeq \frac{\beta^{1/2}a^2}{hc_s}$$

Elastic tension acting in the polyion, $t(r)/k_B T \simeq \mathrm{d}r/a^2\mathrm{d}n$, in the salt-dominated external sublayer is balanced by the osmotic stretching force

$$\frac{f_\perp^{II}(r)}{k_B T} = s(r)\Delta\Pi(r)/k_B T \simeq \frac{hr\beta^2 c(r)^2}{a^3 c_s}$$

to give (taking into account eqn (10)) for the polymer density profile,

$$c_{II}(r) \simeq a^{4/3}\frac{{c_s}^{1/3}}{(\beta hr)^{2/3}}, \qquad (22)$$

and size $\xi(r)$ of the elastic blob,

$$\xi_{II}(r) \simeq k_B T/t(r) \simeq \left(\frac{ahc_s}{\beta^2}r\right)^{1/3} \qquad (23)$$

By normalizing the polymer density profile,

$$na^3 \simeq \int_{r_I}^{D_{II}} c_{II}(r) rh\mathrm{d}r,$$

one finds the brush thickness $D_{II} \gg r_I$ in the salt-dominance regime II,

$$D_{II} \simeq a^{5/4}\left(\frac{\beta^2}{c_s}\right)^{1/4}\frac{n^{3/4}}{h^{1/4}} \qquad (24)$$

Using eqn (14) and (15), the ion-induced h-dependent contribution $F_{II,ion}$ to the total electrostatic free energy per chain in regime II is presented as

$$\begin{aligned}\frac{F_{II,ion}}{k_B T} &= \int_a^{D_{II}} \left[c_-(r)\ln\left(\frac{c_-}{c_s}\right) + c_+(r)\ln\left(\frac{c_+}{c_s}\right)\right] a^{-3}s(r)\mathrm{d}r \\ &\simeq \int_a^{D_{II}} \beta^2 \frac{{c_{II}}^2(r)}{c_s} a^{-3}s(r)\mathrm{d}r \simeq \frac{\beta}{{c_s}^{1/2}}\left(\frac{na}{h}\right)^{1/2}\end{aligned} \qquad (25)$$

The lateral stretching force imposed on the backbone by mobile ions is given by

$$\frac{f_\parallel^{II}}{k_B T} = -\frac{1}{k_B T}\frac{\partial F_{II,ion}}{\partial h} \simeq \frac{a^{1/2}}{h^{3/2}}\left(\frac{\beta^2 n}{c_s}\right)^{1/2} \qquad (26)$$

The brush thickness D_{II} in regime II coincides with the $D(c_s)$ dependence obtained in the mean-field approximation without separating intra- and intermolecular interactions between charges on polyions, and we refer to this regime as the classic salt-dominated one.

4.3 Regime III

The salt-dominated regime II lasts until tension in the polyions $t(D_{II})/k_BT \simeq \xi_{II}^{-1}(D_{II})$ becomes equal to tension $t_e/k_BT \simeq \xi_e^{-1} \simeq u^{1/3}\beta^{2/3}$ created by charges in individual polyion, to give

$$c_s^{II} \simeq \frac{a}{nh\beta^{2/3}u^{4/3}} \quad (27)$$

At this point, the area per chain $\Sigma \simeq hD_{II}$ at the outer boundary of the brush becomes equal to $r_D^2(c_s^{II})$, and further increase in $c_s > c_s^{II}$ leads to the formation of an external sublayer formed by segments of unperturbed individual polyions at distances $r > r^{II}$ while chain segments in the inner sublayer with radius r^{II} retain the structure of regime II. Radius $r^{II}(c_s)$ is specified from the equality $s(r) \simeq hr \simeq r_D^2$ to give

$$r^{II} \simeq \frac{a^2}{uhc_s} \quad (28)$$

The size r^{II} of the inner sublayer becomes much smaller than the size $R_e \simeq anu^{1/3}\beta^{2/3}$ of individual polyion when $c_s \gtrsim c_s^{II}$, and the brush retains its thickness

$$D_{III} \simeq R_e \simeq an\beta^{2/3}u^{1/3} \quad (29)$$

in regime III.

Each polyion in regime III is envisioned as a string of R_e/r_D symmetric subunits with size r_D, and an increase in $c_s \gg c_s^{II}$ merely changes the total number R_e/r_D of subunits without changing the polyion size R_e. At length scales below r_D the chain segment retains the structure of an individual polyion in the salt-free solution with actual chain tension $t_0 \cong k_BT/\xi_e$. On length scales larger than r_D, a polyion is envisioned as a chain of symmetric impermeable subunits with size r_D stretched up to its full length, R_e. This conformation of a polymer chain with subunit size r_D is attained if it is exposed to a stretching force larger than $\simeq k_BT/r_D$, *i.e.*, the inverse size of the impermeable subunit of size r_D.

The polymer density profile in regime III is given by

$$c_{III}(r) \simeq \frac{a}{\beta^{2/3}u^{1/3}hr} \quad (30)$$

While the size ξ of the elastic blob for the string of subunits of size r_D remains on the order of r_D

$$\xi_{III} \simeq r_D \quad (31)$$

The stretching force caused by the differential osmotic pressure of mobile ions, decreases in regime III as

$$\frac{f_\perp^{III}}{k_BT} = s(r)\Delta\Pi(r)/k_BT \simeq \frac{\beta^{2/3}}{c_s}\frac{a^2}{u^{2/3}hr} \quad (32)$$

where

$$\Delta\Pi(r)a^3/k_BT \cong \beta^2 c_{III}^2(r)/c_s \cong \frac{\beta^{2/3}}{c_s}\frac{a^4}{u^{2/3}(hr)^2} \quad (33)$$

Notably, the force $f_\perp^{III}$ given by eqn (32) is smaller than $k_BT\xi_e^{-1}$ at distances $r \geq r^{II}$ given by eqn (28), but larger than $k_BTr_D^{-1}$ at $r \cong D_{III} \cong R_e$.

In this regime III,

$$\frac{F_{III,ion}}{k_BT} \simeq \int_a^{D_{III}=R_e} \beta^2\frac{c_{III}^2(r)}{c_s}a^{-3}s(r)\mathrm{d}r \simeq \frac{a\beta^{2/3}}{u^{2/3}hc_s}\ln\left(n\beta^{2/3}u^{1/3}\right) \quad (34)$$

and the lateral stretching force $f_\parallel$ originating due to osmotic pressure of mobile ions is given by

$$\frac{f_\parallel^{III}}{k_BT} = -\frac{1}{k_BT}\frac{\partial F_{III,ion}}{\partial h} \simeq \frac{a\beta^{2/3}}{u^{2/3}c_sh^2} \quad (35)$$

4.4 Regime IV

At salt concentrations reaching the threshold value $c_s = c_s^{III}$, the electrostatic stretching force $f_\perp$ acting at the outermost subunit ($r \simeq R_e$) reduces to $k_BTr_D^{-1}$ to give

$$c_s^{III} \simeq \left(\frac{a}{u^{3/2}nh}\right)^{2/3} \quad (36)$$

At $c_s > c_s^{III}$, the inner sublayer with size r_{IV} retains the structure of the individual polyion in salt-free solution, while the external sublayer exhibits the excluded volume statistics on length scales larger than r_D. The condition

$$hr_{IV}\cdot\Delta\Pi(r_{IV})/k_BT \simeq r_D^{-1} \quad (37)$$

specifies radius

$$r_{IV} \simeq \frac{\beta^{2/3}}{c_s^{3/2}}\frac{a^2}{hu^{7/6}} \quad (38)$$

of the inner sublayer.

In the outer sublayer (*i.e.*, at $r > r_{IV}$), the size of elastic blob is $\xi(r) > r_D$. Let $\xi(r)$ contain $g_D(r)$ subunits with size r_D, so that $\xi(r) \simeq r_Dg_D^{3/5}(r)$. Because each subunit contains $r_D/\xi_e \cong r_D\beta^{-2/3}u^{-1/3}/a$ monomers, the elastic blob contains

$$m(r) = \frac{g_D(r)r_D\beta^{-2/3}u^{-1/3}}{a} \simeq \left(\frac{\xi(r)}{r_D}\right)^{5/3}\frac{r_D\beta^{-2/3}u^{-1/3}}{a} \simeq \frac{\xi^{5/3(r)}}{ar_D^{2/3}}\beta^{-2/3}u^{-1/3} \quad (39)$$

monomer units to produce polymer volume fraction radial profile

$$c(r) \simeq \frac{m(r)a^3}{\xi(r)hr} \simeq \xi^{2/3}(r)\left(\frac{c_s}{\beta^2}\right)^{1/3}\frac{a^{4/3}}{u^{1/3}hr} \quad (40)$$

Force balance condition

$$s(r)\Delta\Pi(r)/k_BT \simeq hr\frac{\beta^2}{a^3c_s}c^2(r) \simeq \left(\frac{\beta^2}{c_s}\right)^{1/3}\xi(r)^{4/3}\frac{a^{-1/3}}{u^{2/3}hr} \simeq \frac{1}{\xi(r)} \quad (41)$$

gives

$$\xi_{IV}(r) \simeq a^{1/7}\left(\frac{c_s}{\beta^2}\right)^{1/7}(hr)^{3/7}u^{2/7} \quad (42)$$

and

$$c_{IV}(r) \simeq \xi^{2/3}(r)\left(\frac{c_s}{\beta^2}\right)^{1/3}\frac{a^{4/3}}{hr} \simeq \left(\frac{c_s}{\beta^2}\right)^{3/7}\left(\frac{a^2}{hr}\right)^{5/7}u^{-1/7} \quad (43)$$

By normalizing the polymer density profile

$$na^3 \simeq \int_a^{D_{IV}} c_{IV}(r)hr\mathrm{d}r$$

one finds brush thickness D in regime IV,

$$D_{IV} \simeq a^{11/9}\frac{n^{7/9}}{h^{2/9}}\left(\frac{\beta^2}{c_s}\right)^{1/3}u^{1/9} \quad (44)$$

The ion-induced electrostatic free energy contribution

$$\frac{F_{IV,ion}}{k_BT} \simeq \int_a^{D_{IV}}\beta^2\frac{{c_{IV}}^2(r)}{c_s}a^{-3}s(r)\mathrm{d}r \approx \left(\frac{\beta^2}{c_s}\right)^{1/3}n^{4/9}\left(\frac{a}{h}\right)^{5/9}u^{-2/9} \quad (45)$$

and the lateral force applied to the backbone is

$$\frac{f_\parallel^{IV}}{k_BT} = -\frac{1}{k_BT}\frac{\partial F_{IV,ion}}{\partial h} \simeq n^{4/9}\frac{a^{5/9}}{h^{14/9}}\left(\frac{\beta^2}{c_s}\right)^{1/3}u^{-2/9} \quad (46)$$

Subregime $c_s > c_s^*$. In the middle of regime IV at $c_s = c_s^*$, the Debye radius r_D becomes equal to size ξ_e of the electrostatic blob, and at $c_s > c_s^*$, the structure of the electrostatic blob is disrupted. In this subregime, the chain is envisioned as a sequence or subunits with size r_D inside which the chain segments with g monomers and charge $q = \beta g$ exhibit the Gaussian statistics. That is, $g \simeq (r_D/a)^2$ and $q \simeq \beta(r_D/a)^2$. On length scales larger than r_D, polyions exhibit the excluded volume statistics with the second virial coefficient $\tilde{v}_{el} \simeq aq^2{r_D}^2 \simeq \beta^2{r_D}^6/a^3$ of binary interactions between subunits. The elastic blob at distance r from the backbone that contains $m(r)$ monomer units has size

$$\xi(r) \simeq r_D\left(\frac{el}{{r_D}^3}\right)^{1/5}\left(\frac{m(r)}{g}\right)^{3/5} \simeq a^{3/5}\left(\beta^2{r_D}^2\right)^{1/5}m^{3/5}(r) \quad (47)$$

and the force balance condition

$$f_p(r)/k_BT \simeq hr\left(\beta^2{r_D}^2\right)c^2(r)a^{-5} \simeq hr\left(\beta^2{r_D}^2\right)\left(\frac{m(r)}{\xi(r)hr}\right)^2 a \simeq \xi(r)^{-1} \quad (48)$$

specifies (with the account of eqn (47)) $\xi(r) = \xi_{IV}(r)$. As a result, the polymer density profile $c(r)$ and the brush thickness D remain unchanged and are given by eqn (43) and (44), respectively, and the ion-induced contribution $F_{IV} \simeq W_{IV,1}$ is still specified by eqn (45).

When the Debye radius r_D becomes smaller than the average distance d between charges in volume ${r_D}^3$, *i.e.*, $r_D < d \simeq a^{2/3}(r_D/\beta)^{1/3}$, or, equivalently $c_s > \beta$, then the electrostatic interactions between distal parts of the polyion give rise to the electrostatic virial coefficient $v_{el} \simeq a\beta^2{r_D}^2 < a^3$ of binary monomer–monomer interactions. This does not change the power law dependences for $\xi_{IV}(r)$, D_{IV}, and $F_{IV,ion}$ and in the whole regime VI, the lateral tension $f_\parallel$ is given by eqn (46). Notably, at $c > c^*$ in regime IV the ion-induced contribution to the electrostatic free energy become equal (with an accuracy of numerical prefactor) to the energy of electrostatic repulsions between charged monomers of polyions.

The size of elastic blob $\xi(r)$ in eqn (42) becomes on the order of the lateral distance between neighboring polyions, $(hr)^{1/2}$, at distance

$$r'_{IV} \simeq \frac{a^2}{h}\left(\frac{c_s}{\beta^2}\right)^2u^4 \simeq \frac{a^2}{h}\left(\frac{a^3}{v_{el}}\right)^2 \quad (49)$$

from the backbone. At this point, the elastic blob with size $\xi(r) \simeq a/v_{el}$ lo]ses swelling. At distances $r < r'_{IV}$, the blob size $\xi_{IV}(r) < (hr)^{1/2}$, and the brush retains the structure of regime IV, while at $r > r'_{IV}$, ternary monomer–monomer interactions specify the brush structure and the outer brush sublayer exhibits quasi-neutral behavior with densely packed elastic blobs.

4.5 Regime V

The size of internal sublayer $r'_{IV} \simeq D_{IV}$ when the salt concentration is

$$c_s = c_s^{IV} \simeq \beta^2(nh/a)^{1/3}u^{-5/3}$$

and at $c_s \gg c_s^{IV}$, the inner sublayer with size r'_{IV} decreases, while the outer sublayer with thickness

$$D_V \simeq an^{2/3}\left(\frac{a}{h}\right)^{1/3} \quad (50)$$

constitutes the densely packed system of elastic blobs with size

$$\xi_V(r) \simeq (hr)^{1/2} \quad (51)$$

The polymer density profile in regime V is given by

$$c_V(r) \simeq \frac{a}{\xi_V(r)} \simeq \frac{a}{(hr)^{1/2}} \quad (52)$$

The h-dependent ion-induced electrostatic free energy contribution

$$\frac{F_{V,ion}}{k_BT} \simeq \int_{r'_{IV}}^{D_V}\frac{\beta^2}{c_s}{c_V}^2(r)a^{-3}s(r)\mathrm{d}r \simeq \left(\frac{\beta^2}{c_s}\right)n^{2/3}\left(\frac{a}{h}\right)^{1/3} \quad (53)$$

is weaker than the free energy of the ternary non-electrostatic repulsions between monomers,

$$\frac{F_V}{k_BT} \simeq \int\frac{\mathrm{d}r}{\xi_V(r)} \simeq n^{1/3}\left(\frac{a}{h}\right)^{2/3} \gg \frac{F_{V,ion}}{k_BT} \quad (54)$$

and the lateral stretching force

$$\frac{f_\parallel^V}{k_BT} = -\frac{1}{k_BT}\frac{\partial F_V}{\partial h} \simeq n^{1/3}\frac{a^{2/3}}{h^{5/3}} \quad (55)$$

In Table 2 the power law dependences for brush thickness D, polymer density profile $c(r)$, and size of elastic blob $\xi(r)$ are collected as functions of salt concentration c_s (Table 3). Q4

Notably, depending on the values of h and β, some of the discussed above regimes can disappear. In subregime O_1 ($\beta > (hn/a)^{-1/6}$, colored green in Fig. 2b), the brush never enters quasi-neutral regime V upon increasing salt concentration up

Table 2 Power law dependences for PE brush thickness D, size of elastic blob $\xi(r)$, and polymer density profile $c(r)$ in salt-added solution ($l_B \simeq a$)

Regime	D/an	$\xi(r)/a$	$c(r)$
I	$\beta^{1/2}$	$\beta^{-1/2}$	$\beta^{-1/2}a^2/rh$
II	$(\beta^2/c_s)^{1/4}(nh/a)^{-1/4}$	$(a^2\beta^2/c_s rh)^{-1/4}$	$(c_s/\beta^2)^{1/3}(a^2/rh)^{2/3}$
III	$\beta^{2/3}$	$r_D/a \simeq c_s^{-1/2}$	$\beta^{-2/3}\ a^2/rh$
IV	$(a/nh)^{-2/9}(\beta^2/c_s)^{1/3}$	$(rh/a^2)^{3/7}(c_s/\beta^2)^{1/7}$	$(c_s/\beta^2)^{3/7}(a^2/hr)^{5/7}$
V	$(hn/a)^{-1/3}$	$(rh/a^2)^{1/2}$	$(a^2/rh)^{1/2}$

Table 3 Power law dependences for the boundaries between different regimes for PE brush in salt-added solution ($l_B \simeq a$)

Regime	Upper boundary of regime
I	$c_s^{I} \simeq a(nh)^{-1}$
II	$c_s^{II} \simeq a(\beta^{2/3}nh)^{-1}$
III	$c_s^{III} \simeq a^{2/3}(nh)^{-2/3}$
IV	$c_s^{IV} \simeq \beta^2(nh)^{1/3}$
V	1

to $c_s \simeq 1$. In subregime O_2 ($(hn/a)^{-1/6} > \beta > (hn/a)^{-1/2}$, colored pink in Fig. 2b), all five regimes are present, while in subregime O_3 ($(hn/a)^{-1/2} > \beta > (hn/a)^{-2/3}$, colored blue in Fig. 2b), intermediate regimes III and IV disappear, and the cylindrical PE brush demonstrates the behavior predicted earlier in the mean-field framework.[46]

In Fig. 5 we present the asymptotic power law dependences $D(c_s)$ indicated by colors similar to colors of subregimes O_1, O_2, and O_3. As shown from Fig. 4, a mean-field picture of a cylindrical PE brush in salt-added solution (that is, when the intrachain repulsions are not separated from the overall charge–charge interactions) is expected at relatively weak ionization of tethered polyions (blue region in the diagram of states in Fig. 3b). In this range of the system parameters, the concept of an electrostatic blob is not applicable at any salt concentrations c_s.

In Fig. 6 we illustrate the blob structure of the tethered polyions in various regimes of the diagram of states in Fig. 2 and 3.

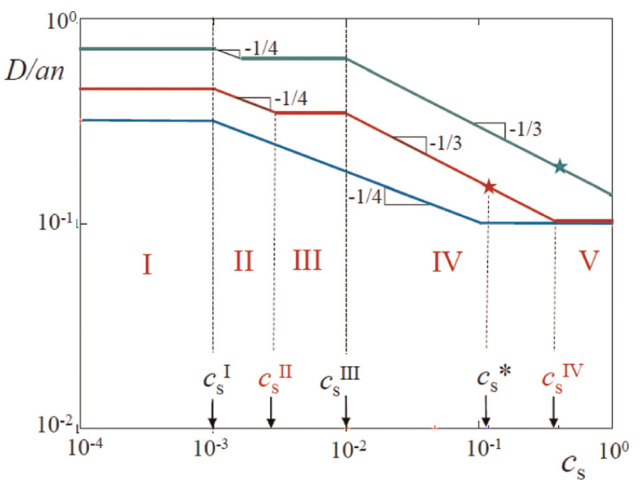

Fig. 5 Reduced thickness D/an of a cylindrical PE brush as a function of salt concentration c_s for fixed $nh/a = 10^3$ (*e.g.*, $n = 200$, $h/a = 5$), and $\beta = 0.5$ (region O_1 in Fig. 4, green lines), $\beta = 0.2$ (region O_2 in Fig. 4, red lines) and $\beta = 0.1$ (region O_3 in Fig. 4, blue lines). Stars indicate the concentration $c_s = c_s^* = \beta^{4/3}(r_D = \xi_e)$ above which the structure of electrostatic blob is disrupted in regime IV. For $\beta = 0.2$ (red lines), salt-dependent boundary concentrations c_s^{II} and c_s^{IV} are shown in red, while salt-independent concentrations c_s^{I}, c_s^{III}, and c_s^* are indicated in black. Different regimes for $\beta = 0.2$ are indicated by red numbers.

5 Discussion

In this study we revisited the original scaling model of PE cylindrical brushes,[37] separating intra- and intermolecular Coulomb repulsions in the tethered polyions.

A previous approach to planar PE brushes[41] has demonstrated that separation of intra- and interchain electrostatic repulsions changes the dependence of the brush thickness $H(c_s)$ in the salt-dominated regime from $H \sim c_s^{-1/3}$ to $H \sim c_s^{-3/7}$. That is, $H(c_s)$ exhibits a sharper dependence on salt concentration c_s than it follows from the model with laterally smeared charges. The change in exponent is attributed to the account of intrachain polyion repulsions that start to manifest themselves after a plateau with $H \simeq R_e \sim c_s^0$ corresponding to size R_e of the individual polyion in a salt-free solution. The role of small ions in the revised scaling model reduces to the creation of the electrostatic force $f_\perp(c_s)$ (due to the differential

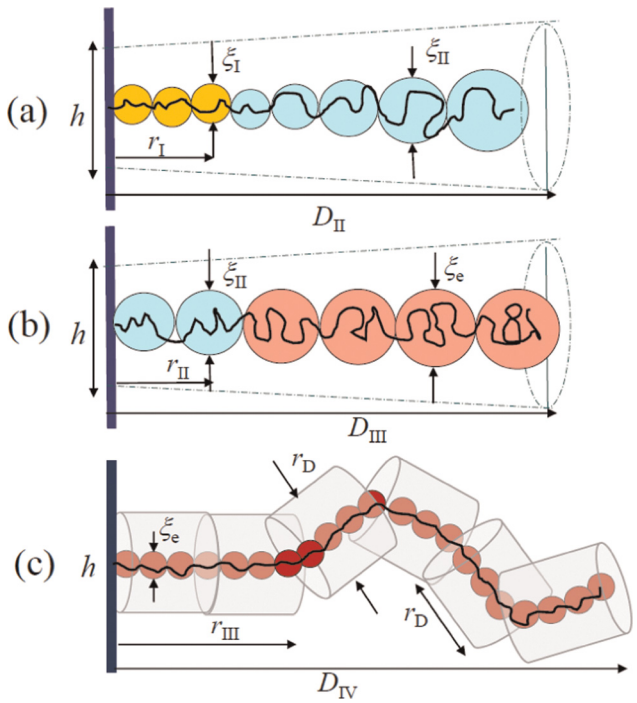

Fig. 6 Schematics of blob structure in tethered polyions in salt-added solution: (a) regime II with $c_s > c_s^{I}$; (b) regime III with $c_s > c_s^{II}$; (c) regime IV with $c_s^{III} < c_s < c_s^*$. The green color indicates blobs in salt-dominated regime II, and the other colors are the same as in Fig. 2 and 3. The degree of ionization is different in schematics (a)–(c) with the maximal value of β in (c).

osmotic pressure of all mobile ions), tending to stretch tethered polyions normally to the grafting surface. An increase in salt concentration c_s leads to a decrease in $f_\perp(c_s)$ and simultaneous decrease in $r_D \sim {c_s}^{-1/2}$. If $f_\perp(c_s)$ reduces below intrinsic tension in the polyion, $\simeq k_BT/\xi_e$, then the intra-chain Coulomb repulsions retain the conformation of an individual polyion with size R_e, independent (in scaling terms) of the salt concentration, c_s. When however $f_\perp(c_s)$ reduces below $\simeq k_BT/r_D$, then the polyion starts to exhibit self-avoiding statistics on length scales larger than the Debye radius, r_D, giving rise to exponent $-3/7$ in the $H(c_s)$ dependence.

A physically similar picture is predicted for the cylindrical PE brush as well. We focused here on the case of a thin cylinder with radius $\rho \ll D$, distance $h \geq a$ between neighboring grafting points, and close to theta-solvent conditions with respect to the van der Waals monomer–monomer interactions. In this case, the scaling model of the molecular brush with a stiff backbone[46] uses the same threshold condition for counterion condensation as for linear polyion with a net linear number charge density $\beta n/h$. That is, the number of condensed in the brush counterions ensures a residual charge density ${l_B}^{-1} \simeq a^{-1}$. Therefore, if $\beta n/h \gg {l_B}^{-1} \simeq a^{-1}$ then the cylindrical PE brush retains the dominant fraction of its counterions and is thereby found in the osmotic regime. In the opposite limit the brush is almost barely charged. The counterion condensation threshold is indicated by red lines in the diagram of states in Fig. 2a and b. Although this condition might be not precisely accurate (see, *e.g.* ref. 47 for a detailed discussion of ion distribution near charged colloids), we use this expression for condensation threshold in the revised model of the cylindrical brush as it provides smooth crossover between PE brush thickness in the osmotic (O) and charged (C) regimes.

In contrast to a planar PE brush in which the polymer density profile does not exhibit a power law dependence as a function of distance r from the surface, the polymer density profile $c(r)$ in a cylindrical PE brush is described by a power law function of r. The value of exponent depends on salt concentration c_s (eqn (18), (22), (30), (30) and (52)). Similarly to a planar PE brush, thickness D of a cylindrical PE brush exhibits a sharper decrease with c_s after passing the plateau with $D \simeq R_e$ (regime III). Here, the exponent in $D(c_s)$ dependence changes from $D \sim {c_s}^{-1/4}$ (classic regime II) to $D \sim {c_s}^{-1/3}$ (regime IV), followed by leveling to $D \sim c_s^0$ (quasi-neutral regime V).

In addition to the brush thickness D and polymer density profile $c(r)$, we have also estimated the lateral tension $f_\parallel$ imposed by polyions on the cylindrical backbone. If the backbone was flexible with a spacer composed of m monomer units, then the equilibrium distance h between grafts would be found from the balance between spacer elasticity and $f_\parallel$.

As we have demonstrated previously in ref. 46, a mean-field model of bottlebrush polyelectrolytes with flexible compatible spacers and side chains provides the scaling expression for the equilibrium distance h between grafts which follows from balancing the backbone restoring force, $f_{el}/k_BT \sim h/a^2m$, and the lateral tension f_{II} imposed by the side chains. The results of ref. 46 remain valid in the osmotic regime I (with eqn (21) for f_{II}), classic salt-dominated regime II (with eqn (26) for f_{II}), and quasi-neutral regime V (eqn (55) for f_{II}), but should be modified in the revised salt-dominated regimes III (eqn (35) for f_{II}) and IV (eqn (46) for f_{II}). In contrast to moderate stretching of backbones in the melt of bottlebrush polymers with relatively long spacers,[48] or even backbone folding in melts of bottlebrush polymers with incompatible main and side chains,[49] polyelectrolyte bottlebrushes exhibit strong stretching in solutions due to the long-range electrostatic interactions.[46] The latter affect not only the local structure (distance h between grafts, and the brush thickness D) but also large scale conformations of bottlebrush polyelectrolytes. We will consider this situation in a separate study.

One of the major parameters of PE brushes that could be varied experimentally is the degree of ionization β of the tethered polyions. While in synthetic PE brushes can be tuned by variations in pH,[50,51] nature uses enzymatic phosphorylation to vary ionization of polyampholytic proteins.[13]

Many synthetic cylindrical PE brushes are created on cellulose nanocrystals (CNCs) (see, *e.g.* the review in ref. 52). Dense grafting of pH-responsive and long polyacrylic acid ligands to CNCs[50] with grafting density up to 0.3 chains per nm^2 allows for experimental systems that could be checked with the scaling model developed in this paper. Unfortunately, in spite of the enormous amount of publications on decorated CNC dispersions, we did not find systematic data on the brush thickness D as a function of the molecular parameters of the tethered ligands.

To relate the scaling model to biological systems, we consider a cylindrical brush formed by neurofilament (NF) proteins. These proteins organize in cylindrical filaments with almost parallel orientation in cytoskeletal networks in axons of neurons. NF proteins labeled as NF-L (light), NF-M (medium) and NF-H (heavy) according to their molecular weights, contain rigid helical domains that co-assemble into a dense cylindrical NF core with radius ρ = 5 nm, and unstructured flexible projection domains (tails) that radiate outward from the core every 2–3 nm. Phosphorylation of serines in lysine-serine-proline (KSP) motifs in long M- and H-tails regulates their ionization, but has no effect on the shortest L-tails due to the absence of KSP repeats in their sequence. Notably, the shortest NF-L proteins can be reconstituted in filaments *in vitro* to give rise to monodisperse cylindrical brushes with a fixed degree of ionization β. If excess negative charge of L-tail (ΔQ_L = 35 at pH = 7) is uniformly smeared over the whole chain with DP n = 142 (in human NF-L), then $\beta = \Delta Q_L/n$ = 0.25. If, however, the segment of approximately 50 amino acid residues (adjacent to the core and almost uncharged) is excluded from consideration, then the rest of the L-tail has a larger degree of ionization, $\beta = \Delta Q_L/(n - 50)$ = 0.38. In both scenarios the NF-L filament can be envisioned as a cylindrical PE brush with approximately 32 projections per core period with length l = 40–45 nm, to give h/a = 3–4 with size a = 0.6 nm of amino acid (aa) residue.[53]

We indicated the location of cylindrical PE brushes with similar structural parameters using a red square in the diagram of states in Fig. 3. That is, in the salt-free solution the NF-L

brush is found in the osmotic regime O in the vicinity of the O_2–O_3 boundary (either below it if $\beta = 0.25$, or above it if $\beta = 0.38$). According to Table 1, the thickness D of the osmotic PE brush is estimated (with the accuracy of the prefactor in the order of unity) as D = 42 nm or 34 nm, respectively. Notably, a more refined SCF theory provides the numerical prefactor ~ 0.5 leading to the corresponding decrease in D to D = 21 nm or 17 nm, respectively. The average volume fraction of counterions cion in the cylindrical brush, estimated as $c_{ion} = 32\Delta Q_L/l\pi D^2$, encompasses the physiological ionic strength ≈ 0.15 M for these two estimates of D. Therefore under physiological conditions, the L-brush is close to the boundary between osmotic and salt-dominated regimes.

The small-angle X-ray scattering (SAXS) in solutions of reconstituted NF-Ls demonstrated that, under close to physiological conditions, the interfilament spacing changed with protein volume fraction Φ as $\Phi^{-1/2}$, indicating thereby parallel orientation of NF-L filaments.[54]

The closest spacing between pure L-filaments detected from the scattering data was 38 nm. Subtracting the sizes of two cores (each with radius ρ = 5 nm), the thickness D of the L-brush was estimated as 14 nm. In a subsequent study[55] reconstituted NF-Ls were subjected to an osmotic pressure to mediate the average distance between filaments. The data demonstrated purely repulsive interactions with force-distance curves consistent with the polyelectrolyte nature of these PE brushes. The interfilament distance d at low compressions gives an estimate for the L-brush thickness, $D = d/2 - \rho$, at different salt concentrations encompassing the physiological ionic strength. An increase in salt concentration c_s from 40 to 240 mM led to the decrease in D from 19 nm to 13 nm. These data are consistent with the theoretical estimates for the thickness D of the L-brush at the boundary between osmotic and salt-dominated regimes, but is insufficient to check the predicted scaling exponent in the $D(c_s)$ dependence.

The *in vitro* scattering data on NF-L filaments were consistent with *in vivo* experiments on transgenic mice with selectively truncated NF-H and NF-M projections.[56,57] Examination of axoplasms indicated that, in mice that lacked both H- and M-tails, the median spacing between neurofilaments was reduced to 30 nm leading to an estimated brush thickness D = 15 nm.

Therefore, application of the PE brush model to cylindrical NF-L filaments leads to a reasonable correspondence between theory and available experiments.

6 Conclusions

In this study we revisited the scaling model of PE cylindrical brushes applicable to charged molecular brushes with rigid backbones, and polymer-decorated nanorods. We demonstrated that separation of intra- and inter-molecular repulsions between strongly charged tethered polyions (subregimes O_1 and O_2 in the diagram of states in Fig. 2b) leads to additional salt-controlled subregimes, and modification of the exponent in the classic power law dependence of the brush thickness $D(c_s)$. For relatively weakly charged polyions (subregime O_3 in the diagram of states in Fig. 2b), a classic picture of the cylindrical PE brush with three consecutive regimes (osmotic, salt-dominated, and quasi-neutra) is not changed.

Conflicts of interest

■■■■ Q6

Acknowledgements

This work was supported by Russian Science Foundation grant 20-13-00270. Q7

References

1 S. S. Sheiko, B. S. Sumerlin and K. Matyjaszewski, Cylindrical molecular brushes: Synthesis, characterization and properties, *Prog. Polym. Sci.*, 2008, **33**, 759–785.
2 R. Verduzco, X. Li, S. L. Pesek and G. E. Stein, Structure, function, self-assembly of bottlebrush copolymers, *Chem. Soc. Rev.*, 2015, **44**, 2405–2420.
3 J. Rzayev, Molecular Bottlebrushes: New Opportunities in Nanomaterials Fabrication, *ACS Macro Lett.*, 2012, **1**, 1146–1149.
4 H. Liang, S. S. Sheiko and A. V. Dobrynin, Supersoft Polymer Networks with Brushlike Strands, *Macromolecules*, 2018, **51**, 638–645.
5 S. Nian, H. Lian, Z. Gong, M. Zhernenkov, J. Qin and L.-H. Cai, Molecular Architecture Directs Linear-Bottlebrush-Linear Triblock Copolymers to Self-Assemble to Soft Reprocessable Elastomers, *ACS Macro Lett.*, 2019, **8**, 1528–1534.
6 J. Yuan; A. H. E. Müller; K. Matyjaszewski and S. Sheiko, in *Polymer Science: A Comprehensive Reference*, ed.-in-Chief K. Matyjaszewski and M. Möller, Elsevier, Amsterdam, 2012.
7 G. Xie, M. R. Martinez, M. Olszewski, S. S. Sheiko and K. Matyjaszewski, Molecular Bottlebrushes as Novel Materials, *Biomacromolecules*, 2019, **20**(1), 27–54.
8 M. Vatankhah-Varnosfaderani, A. N. Keith, Y. Cong, H. Liang, M. Rosenthal, M. Sztucki, C. Clair, S. Magonov, D. A. Ivanov, A. V. Dobrynin and S. S. Sheiko, Chameleon-like elastomers with molecularly encoded strain-adaptive stiffening and coloration, *Science*, 2018, **359**(6383), 1509–1513.
9 S. S. Sheiko and A. V. Dobrynin, Architectural Code for Rubber Elasticity: from Supersoft to Superfirm Materials, *Macromolecules*, 2019, **52**, 7531–7546.
10 A. L. Liberman-Martin, C. K. Chu and R. H. Grubbs, Application of Bottlebrush Block Copolymers as Photonic Crystals, *Macromol. Rapid Commun.*, 2017, **38**, 1700058.
11 D. P. Song, T. H. Zhao, G. Guidetti, S. Vignolini and R. M. Parker, Hierarchical Photonic Pigments *via* the Confined Self-Assembly of Bottlebrush Block Copolymers, *ACS Nano*, 2019, **13**, 1764–1771.

12 J. Aggrecan Dudhia, aging and assembly in articular cartilage, *CMLS, Cell. Mol. Life Sci.*, 2005, **62**, 2241–2256.

13 E. Fuchs and D. W. Cleveland, A Structural Scaffolding of Intermediate Filaments in Health and Disease, *Science*, 1998, **279**, 514–519.

14 B. Button, L. Cai, C. Ehre, M. Kesimer, D. B. Hill, J. K. Sheehan, R. C. Boucher and M. Rubinstein, A Periciliary Brush Promotes the Lung Health by Separating the Mucus Layer from Airway Epithelia, *Science*, 2012, **337**, 937–941.

15 E. B. Zhulina, S. S. Sheiko and O. V. Borisov, Solution and Melts of Barbwire Bottlebrushes: Hierarchical Structure and Scale-Dependent Elasticity, *Macromolecules*, 2019, **52**(4), 1671–1684.

16 L. Feuz, F. A. M. Leermakers, M. Textor and O. Borisov, Bending rigidity and induced persistence length of molecular bottle brushes: A self-consistent-field theory, *Macromolecules*, 2005, **38**, 8891–8901.

17 X. Ma, Y. Z. Yang, L. Zhu, B. Zhao, P. Tang and F. Qiu, Binary mixed homopolymer brushes grafted on nanorod particles: A self-consistent field theory study, *J. Chem. Phys.*, 2013, **139**, 214902.

18 M. Saariaho, O. Ikkala, I. Szleifer, I. Erukhimovich and G. Ten Brinke, On lyotropic behavior of molecular bottlebrushes: A Monte Carlo computer simulation study, *J. Chem. Phys.*, 1997, **107**, 3267–3276.

19 M. Saariaho, I. Szleifer, O. Ikkala and G. ten Brinke, Extended conformations of isolated molecular bottlebrushes: Influence of side-chain topology, *Macromol. Theory Simul.*, 1998, **7**, 211–216.

20 A. Subbotin, M. Saariaho, O. Ikkala and G. Ten Brinke, Elasticity of comb copolymer cylindrical brushes, *Macromolecules*, 2000, **33**, 3447–3452.

21 S. Elli, F. Ganazzoli, E. G. Timoshenko, Y. A. Kuznetsov and R. Connolly, Size and persistence length of molecular bottlebrushes by Monte Carlo simulations, *J. Chem. Phys.*, 2004, **120**, 6257–6267.

22 P. E. Theodorakis, H.-P. Hsu, W. Paul and K. Binder, Computer simulation of bottle-brush polymers with flexible backbone: Good solvent versus theta solvent conditions, *J. Chem. Phys.*, 2011, **135**, 164903.

23 Z. Cao, J.-M. Y. Carrillo, S. S. Sheiko and A. V. Dobrynin, Computer Simulations of Bottle Brushes: From Melts to Soft Networks, *Macromolecules*, 2015, **48**, 5006–5015.

24 H.-P. Hsu, W. Paul, S. Rathgeber and K. Binder, Characteristic Length Scales and Radial Monomer Density Profiles of Molecular Bottle-Brushes: Simulation and Experiment, *Macromolecules*, 2010, **43**, 1592–1601.

25 H.-P. Hsu, W. Paul and K. Binder, Standard Definitions of Persistence Length Do Not Describe the Local'' Intrinsic'' Stiffness of Real Polymer Chains, *Macromolecules*, 2010, **43**, 3094–3102.

26 E. B. Zhulina, S. S. Sheiko and O. V. Borisov, Polymer Networks Formed by Molecular Brushes: Scaling Theory, *Polym. Sci., Ser. A*, 2019, **61**(6), 799–804.

27 E. B. Zhulina and O. V. Borisov, Bottlebrush polymer gels: architectural control over swelling and osmotic bulk modulus, *Soft Matter*, 2022, **18**(6), 1239–1246.

28 F. Vashahi, M. R. Martinez, E. Dashtimoghadam, F. Fahimpour, A. N. Keith, E. A. Bersenev, D. A. Ivanov, E. B. Zhulina, K. Matyjaszewski, M. Vatankhah-Varnosfaderani and S. S. Sheiko, Injectable hydrogels with tissue-adaptive gelation and mechanical properties, *Sci. Adv.*, 2022, **8**(3), eabm2469.

29 F. Uhlik, O. V. Rud, O. V. Borisov and E. B. Zhulina, Hairy gels: a computational study, *Gels*, 2022, **8**(12), 793–17. Q8 Q9

30 E. Mohammadi, S. Y. Joshi and S. A. Deshmukh, A review of computational studies of bottlebrush polymers, *Comput. Mater. Sci.*, 2021, **199**, 110720.

31 L. J. Qu, X. G. Jin and Q. Liao, Numerical self-consistent field theory of cylindrical polyelectrolyte brushes, *Macromol. Theory Simul.*, 2009, **18**, 162–170.

32 Q.-H. Hao, Q. Chen, Z. Zheng, L.-Y. Liu, T.-J. Liu, X.-H. Niu, Q.-G. Song and H.-G. Tan, Molecular dynamics simulations of cylindrical polyelectrolyte brushes in monovalent and multivalent salt solutions, *J. Theor. Comput. Chem.*, 2016, **15**(3), 1650026.

33 P. A. Pincus, Colloid stabilization with grafted polyelectrolytes, *Macromolecules*, 1991, **24**, 2912–2919.

34 R. Ross and P. A. Pincus, The polyelectrolyte brush: poor solvent, *Macromolecules*, 1992, **25**, 2177–2183.

35 O. V. Borisov, T. M. Birshtein and E. B. Zhulina, Collapse of Grafted Polyelectrolyte Layer, *J. Phys. II*, 1991, **1**(5), 521–526.

36 O. V. Borisov, E. B. Zhulina and T. M. Birshtein, Diagram of States of Grafted Polyelectrolyte Layer, *Macromolecules*, 1994, **27**(17), 4795–4803.

37 E. B. Zhulina and O. V. Borisov, Polyelectrolytes Grafted to Curved Surfaces, *Macromolecules*, 1996, **29**, 2618–2626.

38 K. Bohinc, G. V. Bossa and S. May, Incorporation of ion and solvent structure into mean-field modeling of the electric double layer, *Adv. Colloid Interface Sci.*, 2017, **249**, 220–233.

39 A. V. Dobrynin and M. Rubinstein, Theory of polyelectrolytes in solutions and at surfaces, *Prog. Polym. Sci.*, 2005, **30**(11), 1049–1118.

40 D. J. Sandberg, J.-M. Y. Carrillo and A. V. Dobrynin, Molecular Dynamics Simulations of Polyelectrolyte Brushes: From Single Chains to Bundles of Chains, *Langmuir*, 2007, **23**, 12716–12728.

41 E. B. Zhulina and M. Rubinstein, Ionic Strength Dependence of Polyelectrolyte Brush Thickness, *Soft Matter*, 2012, **8**(36), 9376–9383.

42 O. V. Borisov and E. B. Zhulina, Structure of Weakly Charged Polyelectrolyte Brushes: Monomer Density Profiles, *J Phys. II*, 1997, **7**(3), 449–458.

43 R. C. Ball, J. F. Marco, S. T. Milner and T. A. Witten, Polymers grafted to a convex surface, *Macromolecules*, 1991, **24**, 693–703.

44 V. A. Belyi, Exclusion zone of convex brushes in the strong-stretching limit, *J. Chem. Phys.*, 2004, **121**(13), 6547.

45 O. V. Borisov, E. B. Zhulina, F. A. M. Leermakers, M. Ballauff and A. H. E. Müller, Conformations and solution properties

of star-branched Polyelectrolytes, *Adv. Polym. Sci.*, 2011, **241**, 1–55.
46 O. V. Borisov and E. B. Zhulina, Conformations of polyelectrolyte molecular brushes: A mean-filed theory, *J. Chem. Phys.*, 2018, **149**, 184904.
47 Q. Tang and M. Rubinstein, Where in the world are condensed counterions?, *Soft Matter*, 2022, **18**, 1154–1173.
48 J. Paturej, S. S. Sheiko, S. Panyukov and M. Rubinstein, Molecular structure of bottlebrush polymers in melts, *Sci. Adv.*, 2016, **2**, e1601478.
49 S. Nian, B. Huang, G. Freychet, M. Zhernenkov and L.-H. Cai, Unexpected Folding of Bottlebrush Polymers in Melts, *Macromolecules*, 2023, **56**, 2551–2559.
50 J. Majoinen, A. Walther, J. R. McKee, E. Kontturi, V. Aseyev, J. M. Malho, J. Ruokolainen and O. Ikkala, Polyelectrolyte Brushes Grafted from Cellulose Nanocrystals Using Cu-Mediated Surface-Initiated Controlled Radical Polymerization, *Biomacromolecules*, 2011, **12**(8), 2997–3006.
51 K. H. M. Kan, J. Li, K. Wijesekera and E. D. Cranston, Polymer-Grafted Cellulose Nanocrystals as pH-Responsive Reversible Flocculants, *Biomacromolecules*, 2013, **14**, 3130–3139.
52 Z. Zhang, G. Sebe, Y. Hou, J. Wang, J. Huang and G. Zhou, Grafting polymers from cellulose nanocrystals *via* surface-initiated atom transfer radical polymerization, *J. Appl. Polym. Sci.*, 2021, **138**, e51458.
53 E. B. Zhulina and F. A. M. Leermakers, On Polyelectrolyte Brush Model of Neurofilaments, *Soft Matter*, 2009, **5**(15), 2836–2840.
54 J. B. Jones and C. R. Safinya, Interplay between Liquid Crystalline and Isotropic Gels in Self-Assembled Neurofilament Networks, *Biophys. J.*, 2008, **95**, 823–835.
55 R. Beck, J. Deek, J. B. Jones and C. R. Safinya, Gel-expanded to gel-condensed transition in neurofilament networks revealed by direct force measurements, *Nat. Mater.*, 2009, **9**(1), 40–46.
56 M. V. Rao, M. L. Garcia, Y. Miyazaki, T. Gotow, A. Yuan, S. Mattina, C. M. Ward, N. A. Calcutt, Y. Uchiyama, R. A. Nixon and D. W. Cleveland, Gene replacement in mice reveals that the heavily phosphorylated tail of neurofilament heavy subunit does not affect axonal caliber or the transit of cargoes in slow axonal transport, *J. Cell Biol.*, 2002, **158**, 681–693.
57 M. L. Garcia, C. S. Lobsiger, S. B. Shah, T. J. Deerinck, J. Crum, D. Young, C. M. Ward, T. O. Crawford, T. Gotow, Y. Uchiyama, M. H. Ellisman, N. A. Calcutt and D. Cleveland, NF-M is an essential target for the myelin-directed ''outside-in'' signaling cascade that mediates radial axonal growth, *J. Cell Biol.*, 2003, **163**, 1011–1020.

Dear Author

Please use this PDF proof to check the layout of your article. If you would like any changes to be made to the layout, you can leave instructions in the online proofing interface. First, return to the online proofing interface by clicking "Edit" at the top of the page, then insert a Comment in the relevant location. Making your changes directly in the online proofing interface is the quickest, easiest way to correct and submit your proof.

Please note that changes made to the article in the online proofing interface will be added to the article before publication, but are not reflected in this PDF proof.